AD-A094 158 CATHOLIC UNIV OF AMERICA WASHINGTON DC DEPT OF PHYSICS F/G 20/13
PHASE DIAGRAMS OF A SIMPLE H-BONDED LATTICE GAS OBTAINED WITH T--ETC(U)
JAN 81 E VAN ROYEN, P H MEIJER N00014-78-C-0518
UNCLASSIFIED TR-4 NL

1 OF 1
AD A
094158

END
DATE
FILMED
2-81
DTIC

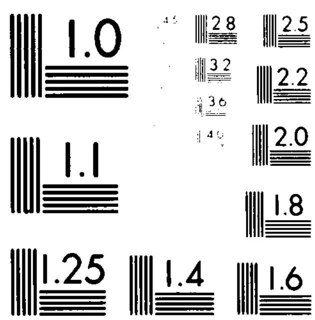

MICROCOPY RESOLUTION TEST CHART

Technical Report 4

Eddy van Royen

and Paul H. E. Meijer

Phase diagrams of a simple H-bonded lattice gas obtained with the Cluster Variation Method.

SECURITY CLASSIFICATION OF THIS PAGE (When Data Entered)

REPORT DOCUMENTATION PAGE		READ INSTRUCTIONS BEFORE COMPLETING FORM
1. REPORT NUMBER 4	2. GOVT ACCESSION NO. AD-A094156	3. RECIPIENT'S CATALOG NUMBER
4. TITLE (and Subtitle) (6) Phase Diagrams of a Simple H-bonded Lattice Gas Obtained With The Cluster Variation Method.		5. TYPE OF REPORT & PERIOD COVERED (9) Technical Report.
		6. PERFORMING ORG. REPORT NUMBER
7. AUTHOR(s) (10) Eddy van Royen Paul H. E. Meijer	(14) TR-4	8. CONTRACT OR GRANT NUMBER(s) (15) ONR N00014-78-C-0518
9. PERFORMING ORGANIZATION NAME AND ADDRESS Physics Department The Catholic University of America Washington, D. C. 20064		10. PROGRAM ELEMENT, PROJECT, TASK AREA & WORK UNIT NUMBERS (12) 38
11. CONTROLLING OFFICE NAME AND ADDRESS Office of Naval Research Arlington, Va. 22217	(11)	12. REPORT DATE Jan [redacted] 81
		13. NUMBER OF PAGES 38
14. MONITORING AGENCY NAME & ADDRESS (if different from Controlling Office)		15. SECURITY CLASS. (of this report) Unclassified
		15a. DECLASSIFICATION/DOWNGRADING SCHEDULE

16. DISTRIBUTION STATEMENT (of this Report)

This document has been approved for public release and sale; its distribution is unlimited.

17. DISTRIBUTION STATEMENT (of the abstract entered in Block 20, if different from Report)

18. SUPPLEMENTARY NOTES

19. KEY WORDS (Continue on reverse side if necessary and identify by block number)

Watermodel, Phase diagram, hydrogen bonding, triplepoint, supercooling, 180° rule, terminal points of metastability.

20. ABSTRACT (Continue on reverse side if necessary and identify by block number)

We evaluate the Bell-lattice-model for water by exploring the parameter space by means of the Cluster Variation method of Kihuchi. We use ten order parameters to describe the different occupation of tetrahedr-ons in the lattice, with and without hydrogen bonds. The phase diagrams are represented in the density-temperature plane and in the pressure temperature plane. An explanation is given as to why there are first order terminal points in the metastable region. We discuss the 180°-rule and display the ratios of hydrogen bonded pairs versus non-hydrogen bonded pairs.

DD FORM 1 JAN 73 1473 EDITION OF 1 NOV 65 IS OBSOLETE
S/N 0102-014-6601

076432

SECURITY CLASSIFICATION OF THIS PAGE (When Data Entered)

ABSTRACT

We evaluate the Bell-lattice-model for water by exploring the parameter space by means of the Cluster Variation method of Kihuchi. We use ten order parameters to describe the different occupation of tetrahedrons in the lattice, with and without hydrogen bonds. The phase diagrams are represented in the density-temperature plane and in the pressure temperature plane. An explanation is given as to why there are first order terminal points in the metastable region. We discuss the 180°-rule and display the ratios of hydrogen bonded pairs versus non-hydrogen bonded pairs.

1. Introduction

We study the Bell[1)] potential for the lattice model of water using the complete cluster variation method. The basic lattice is a bcc lattice and the sites are occupied by oxygen atoms. The hydrogen atoms are oriented along the lines connecting the neighboring atoms. Since the bond angle between two hydrogen atoms is approximately 104°, the hydrogen atoms should lie along those two body diagonals that make the largest angles. This is accomplished by assigning appropriate weight factors. The complete set of tetrahedral configurations, as well as all the sub-clusters, is given in reference 2. We will refer to this model as JWAT for "Junior" Water.

Rather than use the 10 clusters, with the constraint that the total probability should be one, we prefer to introduce the nine independent correlation functions: i.e. all completely occupied clusters and subclusters. (Table 1) All other configuration probabilities can be written as a linear function of these above defined correlation functions.

$$p_i = C_i + \sum_{j=1}^{9} R_{ij} g_j$$

There are 18 configurational probabilities. The factors C_i and R_{ij} are given in Table 2. If the configuration is empty C_i is one, otherwise it is zero. the coefficient R can be obtained from the CR-table in reference 2, by an inversion.

There is an important technical point to mention. In the cluster-variation method one can express each subcluster as a linear combination of larger (sub)clusters. For instance, if on a given point the molecule is oriented in one of the 12 possible ways, this will determine whether this same molecule as partner in a pair, can, or cannot, be hydrogen

bonded. That means a specific choice is made as to whether the linear combination of the y's will contain y_4 (the pair without H-bonding) or y_5 (the pair with H-bonding). In the JWAT model this is not done, instead a linear combination, or average, of these two options is taken. This average is taken with certain combinatorial factors in accordance with the so-called ice rules. The fact that we did not specify the orientation of the molecules will keep the number of cluster variables low, but it will oversimplify the entropy expression and it will of course bar us from any information about the possible rotational ordering of the molecules.

A second simplification we use in the JWAT - model is the half-filled state, i.e. density approximately one half. In this model we find this state at low temperatures by adjusting the energy parameters. Such a state refers to preferred occupation of those clusters that, for a given range of values for the chemical potential, have two sites occupied. It is not specified as to which two out of four sites are occupied, the model again takes an average over two options. 2. Interaction parameters

The lattice model contains three parameters:

e_p the pair interaction between nearest neighbors when they are not hydrogen bonded.

e_H the additional pair energy between two neighboring molecules when they are hydrogen bonded.

e_{nnn} the repulsive next-nearest neighbor interaction.

The first two energies are attractive; the symbol stands for the absolute value of a negative quantity. All energies are expressed in units k_B and hence have the dimension of a temperature.

The absolute values of the interactions are only important for scaling purposes. Using the principle of corresponding states the topology of the phase diagram depends only on a reduced set of interaction parameters. Generally one divides by the largest (i.e. mostly the nearest neighbor interaction) parameter. In the case of the water-model one has the choice between e_p, or e_H (as Bell used) or $e_p + e_H$, the total binding energy of a hydrogen bonded pair. We prefer the first choice.

In fig. 1 and 2 the potential diagrams for the first two cases are drawn, together with the values and mnemonics of the actual potentials for which computations have been performed. The precise values are collected in Table 3. Potential 10 is the same as potential 16 without hydrogen bond energy. Potentials 16 and 17 have been treated in an extended mean field model by Bell and Salt.[3] (our potential 16 is slightly different due to rounding errors; Bell and Salt have $e_p/e_H = 1.45$ and we have $e_p/e_H = 1.450666...$)

There is a general limitation on the choice of potentials, determined by our request that the intermediate state exists. We calculate the generalized pressure from

$$P \equiv p v_0 = \rho \frac{\partial f}{\partial \rho} - f.$$

and for T = 0 there are three states possible: $\rho = 0$ (vacuum) with P = 0, $\rho = 1/2$ (open ice) with $P + 1/2\mu + e_p + e_h$ and $\rho = 1$ (closed packed) with $P + \mu + 4e_p + 2e_h - 3e_{nnn}$. If we plot P at T= 0 (compare fig. 3) we find three possible transitions at

$$\mu_0 = -2(e_p + e_H) \qquad (\text{vac. to open})$$
$$\mu_1 = -4(e_p + 2e_H - 3e_{nnn}) \qquad (\text{c.p. to vac.})$$
$$\mu_{eq} = -16e_p + 2e_H - 6e_{nnn}) \qquad (\text{open to c.p.})$$

In order to obtain a stable intermediate phase we need

$$P_{eq} = \frac{1}{2}(\mu_{eq} - \mu_0) = -2e_p + 3e_{nnn} \geq 0$$

this leads to the "forbidden" area in figures 1 and 2. The values of μ_{eq}, μ_0, P_{eq}, μ_1 are given in Table 3.

The value of the hydrogen bonding parameter does not come in the above condition, since we compare perfect open ice with the close packed phase. The energy difference between c.p. and open is given by two more nearest neighbor bonds and three more next-nearest neighbor bonds as can be found from an inspection of the lattice structure when it is either half occupied (diamond lattice) or fully occupied (bcc). The hydrogen bond energy <u>does</u> come into play in the $P(\mu)$ lines for each of the regions below and above P_{eq}, i.e. is in the open and in the c.p. section separately.

3 <u>The entropy at zero temperature</u>

Since in the JWAT model no sublattices are introduced, and no orientational effects are considered, except for the hydrogen bonding, the open and closepacked ices cannot be treated completely correctly by this model. In order to estimate the difference in entropy at low temperature between the various models we computed the entropy for c.p. and open in JWAT. The open ice structure in the JWAT model can be associated with the case that all tetrahedra are in the configuration 4 in reference 2 (or 24 in Table 2).

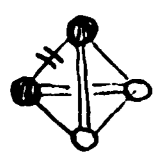

$$p = 1/72 \; ; \; \eta = 6$$

This cluster has multiplicity 72: 4 due to the distributions of the hydrogen bond on the four nearest neighbor edges of the tetrahedron, and 18 because

of the orientational multiplicity of the hydrogen bond.

The correlation functions of the subclusters are now:

$p_{16} = 1/48$; $p_{20} = 1/72$; $p_{12} = 1/24$; $p_{11} = 1/4$; $p_{12} = 1/48$; $p_3 = 1/72$; $p_{10} = 1/2$ and $p_1 = 1/24$.

Substituting this in the expression for the entropy in units k_B:

$$-S = \sum \eta_i g_i p_i \ln p_i$$

where η_i are the Kikuchi numbers, g_i the (total) weight factors and the sum is over all contributing clusters. The result is:

$$S'_{open} = (1/2) \ln 3 - 4 \ln 2 \approx -2.2232$$

The close packed state results if all tetrahedra are in configuration 8 in ref 2 (or number 9 in table 1).

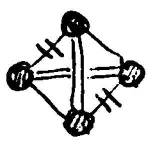

$$p = 1/648 \; ; \; \eta = 6$$

the value of the subclusters is now: $p_6 = 1/143$; $p_4 = 1/144$; $p_2 = 1/252$; $p_3 = 1/36$ and $p_1 = 1/2$. This leads to an entropy

$$S_{cp} = -12 \ln 2 + \ln 3 + 2 \ln 7 \approx -3.3273$$

The absence of a proper two-sublattice description in the JWAT-model, we obtain a rather large negative value of the entropy of these two phases. The result is that the pressure, as given by

$$P = \mu \rho - E + kTS$$

will also be much lower than it would be if the entropy was given correctly. Hence the open and close packed ice phases are underestimated in this model, compared to the liquid/vapour - i.e. the disordered phases. This is most clearly seen by comparing the two sublattice phase diagrams for potentials 12

and 17 with their JWAT counterparts.

It is furthermore interesting to compare the ground state entropy with the results obtained by Bell. Starting with his equation 3.4, i.e.

$$S = -\ln g = -\ln g_o + N \sum_{i=1}^{10} g_i w_i \ln w_i$$

where w_i are representing the ten tetrahedrons, g_i their weight factors and g_o given by:

$$\ln g_o = 3N \left\{ \rho \ln \frac{\rho}{12} + (1-\rho) \ln (1-\rho) \right\}$$

Translated in our language, he took for the Kikuchi numbers the values: 1 for the tetrahedrons and -3 for the points. (and all others zero). That is he considered a collection of N tetrahedrons which overlap only with their vertices, hence $4N$ points are substracted from the N point terms. The systematic procedure of the CVM is to consider all N tetrahedrons that fill the space completely. These overlap with triangles, second neighbors, first neighbors and point sites and thus is taken into account by:

$$S = 6\, S_{tet} - 12\, S_{tr} + 3\, S_{nnn} + 4\, S_{nn} - S_p$$

rather than

$$S = S_t - 3\, S_p$$

as in Bell. It turns out that the large negative contribution comes from the triangular term $-12\ S_{tr}$. For comparison we give also the numerical values of the entropy as obtained by Bell's expression.

$$S_{open} = -3 \ln 2 + \tfrac{1}{2} \ln 3 \approx -1.53$$
$$S_{cp} = -3 \ln 2 + \ln 3 \approx 0.93$$

Finally we would like to mention that the Pauling estimate for open ice leads to $S_o = 1/2 \ln 3/2 = 0.2027$ and twice that amount for the c.p. state.

4. Description and Comparison of a Number of Potentials; Density-Temperature Phase Diagram.

If we look at the ρ-T plot, the influence of the intermediate state will show up in two different ways. Either we find, at high temperatures a direct transition between the disordered low density state to the close packed state, or we find a transition from the low density state to the intermediate state and subsequently, at somewhat lower temperatures, a transition from the intermediate density state to the close packed state. To make an easy distinction between these two case we will refer to the first case as the one-dome phase diagram, i.e. ρ-T diagram, and to the second as the two-dome diagram.

A second characteristic of the ρ-T plots is the appearance of a "slit", a region near one half density where the ρ is zero to one transition is interrupted by an intermediate state so that the transition now takes place in two steps, one from density near zero to a density somewhat less than a half and one from a density somewhat more than a half to a density almost one. Although this two step process is similar to the two step process described above in the "two dome" diagram, there is an important distinction, i.e. at high temperatures this transition disappears. The point of disappearance is a triple point since three phases are in equilibrium with each other. We will see later that for certain values two triple points, since the above mentioned "slit" does also occur in certain two-dome ρ-T diagrams.

4,1) Two-dome potentials.

Let us start with potentials 12, 15 and 11 that have a relatively large e_{nnn}/e_p and a variable amount of e_H. In potential 12 we have a two-dome (See Fig. 4) structure, i.e. two critical densitites. The low density critical temperature is at 400 K, the high density critical temperature at 350 K. The lower value of the second critical temperature is due to the fact that at these density values the fraction of nearest neighbor bonds that is hydrogen bonded is less, leading to a smaller effective pair interaction.

To obtain the high density transition one needs a higher presure and compared to low density critical temperature this is clarly seen in the P-T plot for this potential (Fig. 5). From this plot it is also clear again that the intermediate phase is open-ended. The upper branch descends and subsequently rises somewhat before it ends in the second critical temperature. This second terminal point causes us to reject this type of phase diagram, since it does not reconcile between this type of result and even a qualitiative comparison between this type of result and the observed diagram for water.

A similar set of figures (Fig. 6 and 7) was obtained for potential 15. At low temperatures it takes considerably more pressure to accomplish the second transistion.

The third potential we want to discuss in this section is number 11. This is still a potential with two domes, but it has a characteristic we will find in many of the one dome potentials: there is a triple point at T_3. Below T_3 the potential develops a "slit", as described above. T_3 lies at

152.8 K. The composite sketch (Fig. 8) of the T-ρ results, gives a second triple point T_3' at lower temperatures. Below this temperature we have two transitions again. In the intermediate region $T_3'<T<T_3$ we have a direct transition from the low to the high density state. All dashed lines are metastable transitions. Please note that the low-to-high transition extends above T_3, but ends in a metastable end point T_M. The accompanying pressure temperature plot is given in Fig. 9. The lower branch 1 is related to T_c^1, the upper branch 2 is related to T_c. The metastable branch that goes up to T_M is just visible above branch number one. The two triple points are on the left.

Finally, we describe potential 18, which is almost a one-dome potential. The density temperature diagram is given in figure 10A qualitatively and in figure 10B quantitatively, but incomplete. The noteworthy difference between figures 10 and 8 is that the metastable states between the two triple points are no longer connected.This means in the P-T plot (see figure 11), that the second branch now consists of two independent parts, one labelled "open/cp" and another labelled liquid (1/2) - liquid (1). This last line extends a little bit below the "vap./liq." line.

At the end of this sub-section we would like to discuss the termination of phase lines in the P-T diagrams. As a rule phase lines can only end in second order critical points (ref. 4) since the double tangent construction at temperatures just below T_c will relate two values of the order paramenter say ρ_1 and ρ_2. If we approach T_c, ρ_1 moves towards ρ_2 and the two will coincide. Not so for a metastable double transition. Imagine a function of at least the sixth order, chosen symmetric for convenience. In fig. 12a we took the central value larger than the two maxima at the left and the right.

We can make two double tangent construction , leading to a transition from ρ_1, to ρ_2 and a second transition from ρ_3 to ρ_4 This is the situation below the triple point. At the triple point, the three maxima are of equal height and the tangents coincide: $\rho_2 = \rho_3$. Above (below) the triple point we deal either with a direct transition from ρ_1 to ρ_4 or with two metastable transitions from ρ_1 to ρ_2 and from ρ_3 to ρ_4, but ρ_2 and ρ_3 appear in the reversed order, i.e.: the tangents cross. This option eventually may disappear (see fig. 12d) when the second derivative in ρ_2 and ρ_3 becomes zero. This is the condition for the terminus of the first order metastable transition. Hence it is incorrect to conclude that if the P-T line ends one is necessarily dealing with a second order transition, at least not for a metastable branch.

4.2 One dome potentials

Potentials 16, 17, 13 and 14 are all of the "one-dome" type, that is there is only one critical point at high temperatures and we find a triple point at lower temperatures, which leads to two phase transitions at a given temperature below this triple point. In the P-T diagram we have a stable vapor-open ice coexisting line and a stable open to close-packed line. Open ice, the state where the density is approximately one half, disappears above the triple point and the only stable coexistence line which is left is the vapor to close packed line, which in this simple model, is indistinguishable from the vapor-liquid line.

Empirically we found that the range of values of e_{nnn} that leads to this topology is found in the area of figure 1 below a line given by

$$e_{nnn}/e_p = 0.028 + 0.009\,(e_H/e_p)$$

and above the horizontal line that guarantees three groundstates, as discussed in section 2.

The general features of the one-dome potential can be seen from 16 and 17, which are almost coinciding. See fig. 13 for the temperature-density plot. This plot does not show that there is a triple point at about 30. Figure 14 is the P-T plot. The same remark holds here; there is a branch at temperatures below 150, the left axis of the figure.

Potential 13 is similar to 16 and 17 but since e_H is larger the rectilinear diameter is more bend to the left as can be seen in figure 15. It also has a triple point but at lower temperatures. In potential 14 the triple point lies higher with respect to the critical point. In this potential we have: $T_c = 480$ and $T_3 = 240$, see figure 16. The relative proximity of T_c and T_3 makes it inviting to compare this potential with real water. The pressure- temperature plot (figure 17) shows an undercooling branch far into the negative pressures. It is strongly indicated from preliminary reports about the work of R. Speedy [5] that such a curve indeed exists in water that is under tension.

4.3 Evolution of one type into the other

Let us focus on potential 18, figure 10A. This diagram is the lynchpin of our considerations. By imagining changes one can obtain all others. At one hand; if the two triple points move towards each other, first we obtain figure 8 (no metastable terminal points in the center section) and eventually figure 4 a pure two-dome phase diagram, because the two triple points will eliminate each other, as can be seen from a succession of P-T curves. At the other hand if the upper triple points moves higher, the two-dome feature

disappears and we obtain a single critical temperature.

5. Behavior around a triple point. A triple point in the P-T plot means that three branches meet in one point. Such encounters are subject to "The 180°-Rule" (see ref. 6). Each line has a metastable extension given by a dotted line in fig. 18 and one way to express the rule is that the extension of line (should always lie between the lines 2 and 3. Our computations satisfy this requirement.

6. The hydrogen bonding

The subcluster variables y_1 to y_4 denote the fraction of empty nearest neighbor pairs, the fraction of nn pairs that are half occupied and half unoccupied, the fraction of pair sites that are both occupied without, respectively with, hydrogen bondingg. It makes more sense t o consider either the ratio between hydrogen bonded pairs and bonded pairs: y_3/x_3.

Plotting of the first ratio is of some advantage since it can easily be checked for its assumption value at low densities:

$$\lim_{\rho \to 0} \frac{y_4}{y_3+y_4} = \frac{\exp(e_H/kT)}{7+\exp(e_H/kT)}$$

since the ration y_4/y_3 approaches the appropriate Boltzmann factor. At higher densities this approximation f ails and as a result of the ice rules the number of hydrogen bonded pairs $y_H = y_4$ compared to the number of non-hydrogen bonded pairs $y_{NH} = y_3$ starts to decrease. Each separately does increase, at higher densities, but y_{NH} increase more rapidly.

At higher densities and lower temperatures the oxygens will make as many hydrogen bonds as possible, at the cost of the non-hydrogen bonded pairs, but eventually this can no longer be done in the dissordered phase and this leads

to instability.

Numerical results for the ration (here plotted as y_N/y_H) are given for a "two dome" potential 12 (see figure 19) and for a "one dome" potential, number 14 (see figure 20). The last case illustrates the description we just gave: The number of y_N at very high densities decreases, but at low temperatures this phase is no longer stable. The stable part is near the half density, in the center of the figure.

We also recall the remark made in the first paragraph of section 4.1, i.e. densities around 3/4 the number of H-bonds is less, than at densities near 1/4, due to poor "accomodation" of the orientation, which leads to a lower critical temperature at the higher density. The most sensible plot is y_H/ρ, but they are not yet available.

7. Phase-diagram at low temperatures.

In this section we consider the behavior of the phase diagram at low, but non-zero, temperatures, in particular potential 14 (see figures 16 and 17). There is an almost horizontal line in the P-T diagram. Below this line we have the vapor phase, above the line we have either the open phase (at low temperatures) or the close packed phase (at temperatures above approximately T=240). The dividing line starts at T=0 and P=260, the "equality" pressure mentioned in section 2. This line, the cp-open transition descends towards the horizontal vapour line and ends at a triple point P_3, T_3. The extension below the axis is a metastable transition.

The descending P-T curve is determined by:

$$\left.\frac{dP}{dT}\right|_{coex} = \frac{\partial P}{\partial \mu}\left.\frac{\partial \mu}{\partial T}\right|_{coex} + \frac{\partial P}{\partial T} = \rho\frac{\Delta S}{\Delta \rho} + S = \frac{S^{(1)}\rho^{(2)} - \rho^{(1)}S^{(2)}}{\rho^{(1)} - \rho^{(2)}}$$

Using the values for the entropy computed in section 3 gives

$$\lim_{T\to 0}\left(\frac{\partial P}{\partial T}\right)_{cx} = 2\ln(4/7) < 0$$

This is not the case in the two orientation-two sublattice model, we will discuss in the next report. The negative slope is due to the fact that S open < $1/2S_{cp}$.

In the origin we have actually two lines starting at P=0: One is the vapor close packed which is metastable up to the triple point and one that is related to the vapor-open transition. The last ends at the triple point, at least its stable part, and carries towards that point with a different slope (180^{o}-rule). A simple calculation confirms this. For vapor-open we have

$$\rho_v = 12\exp(\mu/T)$$

and

$$P = -T(1-\rho)\ln(1-\rho) \approx \rho T$$

At T=0: $\mu_{\text{vap-open}} = \mu_o$ and $\mu_{\text{vap-p}} = \mu_1$. The inequality $\mu_o < \mu_1$ leads to

$$P_{\text{vap-open}} < P_{\text{vap-cp}} \quad (\text{low}\, T)$$

they become equal at the triple point.

Tables

Figures

References

1 G. M. Bell, J. Phys. C Sol. St. Phys. 5, 889, 1972.

2a Paul H. E. Meijer, R. Kikuchi and Pierre Papon: "Phase diagram of water based on a lattice model; I Introductory formulation". (Submitted for publication)

2b Paul H. E. Meijer, R. Kikuchi and E. van Royen: "Improved Lattice Model of Water; II, Two sublattice, two orientation model" (Submitted for publication).

3 G. M. Bell and D. W. Salt, Farad Trans II, 72, 76, 1976.

4 R. B. Griffiths and J. C. Wheeler, Phys. Rev. A 2, 1067 (1974).

5 R. J. Speedy, J. Phys. E 13, 778 (1980).

6 J. C. Wheeler, J. Chem. Phys. 61, 4474 (1974).

#	figure		multiplicity	Kikuchi coeff η
1			12	-1
2	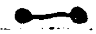	(nn)	126	4
3	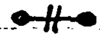	(hydr)	18	4
4		(nnn)	144	3
5		(triangle)	1296	-12
6		(triangle + hydr)	432	-12
7		(tetrah)	11016	6
8		(tetra + hydr)	9072	6
9		(tetr + 2 hydr)	648	6.

Table 1

#	subd.	γ	c	1	2	3	4	5	6	7	8	9
10 1		1	1	-12								
11 2		1	1	-24	126	18						
12 3		24	0	1	$-\frac{21}{2}$	$-\frac{3}{2}$						
13 4		1	1	-24	0	0	144					
14 5		24	0	1	0	0	-12					
15 6		1	1	-36	252	36	144	-1296	-432			
16 7		24	0	1	$-\frac{21}{2}$	$-\frac{3}{2}$	-12	108	36			
17 8		12	0	1	-21	-3	0	108	36			
18 9		144	0	0	0	0	1	-9	-3			
19 10		252	0	0	1	0	0	$-\frac{72}{7}$	$-\frac{12}{7}$			
20 11		36	0	0	0	1	0	0	-12			
21 12		1	1	-48	504	72	288	-5184	-1728	11016	9072	648
22 13		48	0	1	-21	-3	-12	324	108	-918	-756	-54
23 14		288	0	0	0	0	1	-18	-6	$\frac{153}{2}$	63	$\frac{9}{2}$
24 15		72	0	0	0	1	0	0	-24	0	126	18
25 16		504	0	0	1	0	0	$-\frac{144}{7}$	$-\frac{24}{7}$	$\frac{612}{7}$	54	$\frac{18}{7}$
26 17		1728	0	0	0	0	0	0	1	0	$-\frac{21}{2}$	$-\frac{3}{2}$
27 18		5184	0	0	0	0	0	1	0	$-\frac{17}{2}$	$-\frac{7}{2}$	0

Table 2

K	NPOT	EPSILON	W	U2	MU EQ	MU O	P EQ	MU1
1	13	452.40	870.00	312.00	-2582.40	-2644.80	31.20	-2613.60
2	12	650.00	1250.00	600.00	-2800.00	-3800.00	500.00	-3300.00
3	16	544.00	375.00	375.00	-1764.00	-1838.00	37.00	-1801.00
4	17	499.00	554.00	351.00	-1996.00	-2106.00	55.00	-2051.00
5	14	650.00	1250.00	520.00	-3280.00	-3800.00	260.00	-3540.00
6	15	499.00	554.00	460.62	-1338.31	-2106.00	383.85	-1722.15
7	11	544.00	375.00	454.00	-1290.00	-1838.00	274.00	-1564.00
8	18	544.00	375.00	430.00	-1434.00	-1838.00	202.00	-1636.00
9	10	544.00	0.00	375.00	-1014.00	-1088.00	37.00	-1051.00

QUANTITIES REDUCED BY HYDROGENBONDING

1	13	.520		.359	-2.968	-3.040	.036	-3.004
2	12	.520		.480	-2.240	-3.040	.400	-2.640
3	16	1.451		1.000	-4.704	-4.901	.099	-4.803
4	17	.901		.634	-3.603	-3.801	.099	-3.702
5	14	.520		.416	-2.624	-3.040	.208	-2.832
6	15	.901		.831	-2.416	-3.801	.693	-3.109
7	11	1.451		1.211	-3.440	-4.901	.731	-4.171
8	18	1.451		1.147	-3.824	-4.901	.539	-4.363

REDUCED BY EPS

1	13		1.923	.690	-5.708	-5.846	.069	-5.777
2	12		1.923	.923	-4.308	-5.846	.769	-5.077
3	16		.689	.689	-3.243	-3.379	.068	-3.311
4	17		1.110	.703	-4.000	-4.220	.110	-4.110
5	14		1.923	.800	-5.046	-5.846	.400	-5.446
6	15		1.110	.923	-2.682	-4.220	.769	-3.451
7	11		.689	.835	-2.371	-3.379	.504	-2.875
8	18		.689	.790	-2.636	-3.379	.371	-3.007
9	10		0.000	.689	-1.864	-2.000	.068	-1.932

Table 3

August 11, 1980

K	NPOT	e_p	e_H	e_{nnn}	MU EQ	MU O	P EQ	MU 1
1	13	452.40	870.	312.	-2582.	-2644.	31.2	-2613.
2	12	650.	1250.	600.	-2800.	-3800.	500.0	-3300.
3	16	544.	375.	375.	-1764.	-1838.	37.0	-1801.
4	17	499.	554.	351.	-1996.	-2106.	55.0	-2051.
5	14	650.	1250.	520.	-3280.	-3800.	260.0	-3540.
6	15	499.	554.	460.62	-1338.	-2106.	383.8	-1722.
7	11	544.	375.	454.	-1290.	-1838.	274.0	-1564.
8	18	544.	375.	430.	-1434.	-1838.	202.0	-1636.
9	10	544.	0.	375.	-1014.	-1088.	37.0	-1051.

Quantities Reduced by Hydrogenbonding e_H

K	NPOT	e_p	e_H	e_{nnn}	MU EQ	MU O	P EQ	MU 1
1	13	.520		.359	-2.968	-3.040	.035	-3.004
2	12	.520		.480	-2.240	-3.040	.400	-2.640
3	16	1.451		1.000	-4.704	-4.901	.098	-4.802
4	17	.901		.636	-3.602	-3.801	.099	-3.702
5	14	.520		.416	-2.624	-3.040	.208	-2.832
6	15	.901		.831	-2.415	-3.801	.692	-3.108
7	11	1.451		1.211	-3.440	-4.901	.730	-4.170
8	18	1.451		1.147	-3.824	-4.901	.538	-4.362

Reduced by e_p

K	NPOT	e_p	e_H	e_{nnn}	MU EQ	MU O	P EQ	MU 1
1	13		1.923	.689	-5.708	-5.846	.068	-5.777
2	12		1.923	.923	-4.307	-5.846	.769	-5.076
3	16		.689	.689	-3.242	-3.378	.068	-3.310
4	17		1.110	.703	-4.000	-4.220	.110	-4.110
5	14		1.928	.800	-5.046	-5.846	.400	-5.446
6	15		1.110	.923	-2.681	-4.220	.769	-3.451
7	11		.689	.834	-2.371	-3.378	.503	-2.875
8	18		.689	.790	-2.636	-3.378	.371	-3.007
9	10		0.000	.689	-1.863	-2.000	.068	-1.931

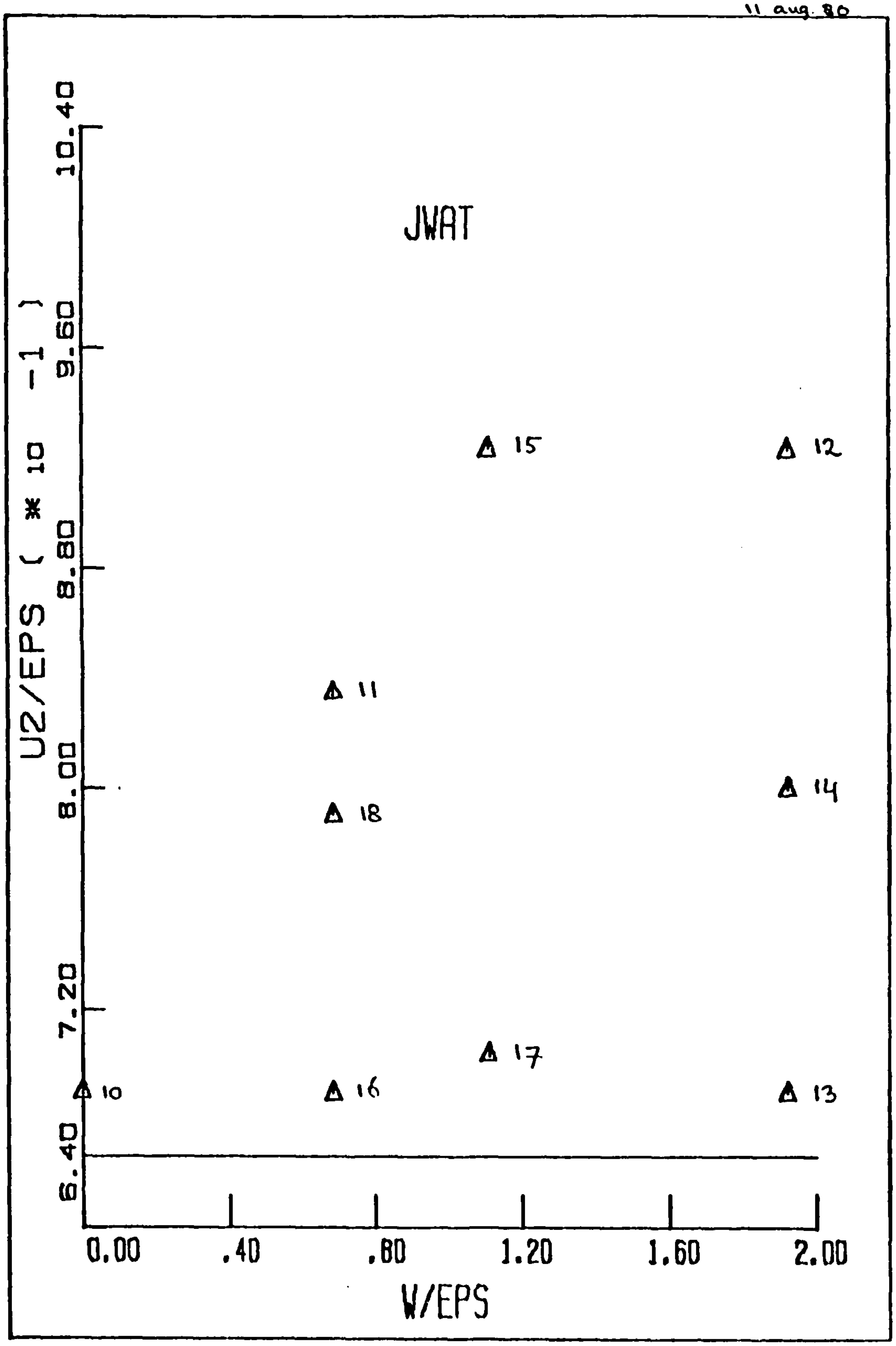

JWAT
U2/EPS (* 10 -1)
10.40
9.60
8.80
8.00
7.20
6.40
W/EPS
0.00
.40
.80
1.20
1.60
2.00
15
12
11
14
18
17
10
16
13

Fig 1

11 aug 80

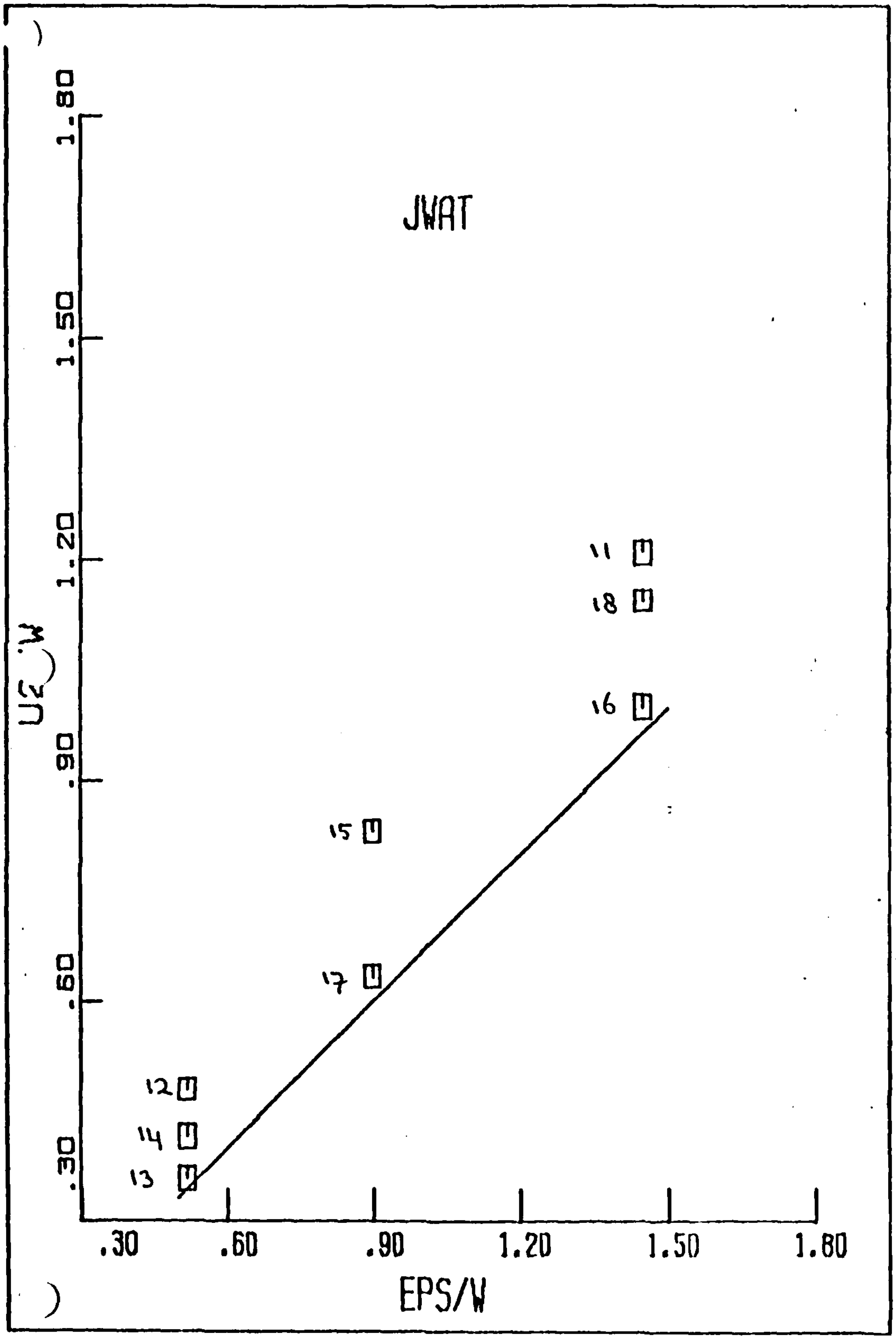

Fig 2

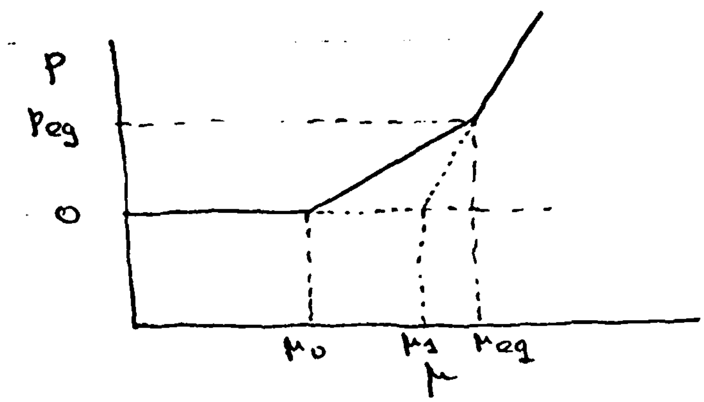
p
peq
0
μ0
μ1
μeq
μ

80/6/2

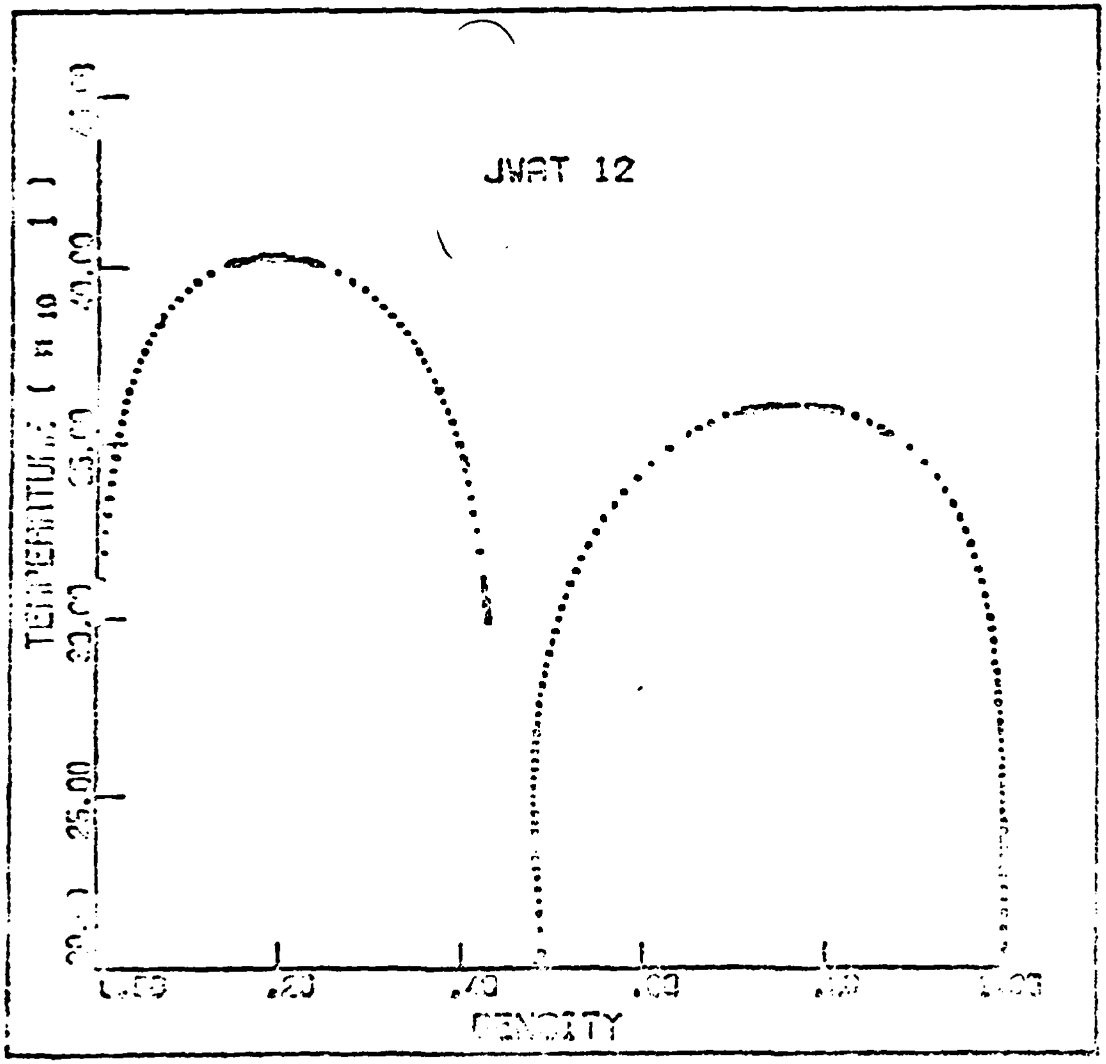

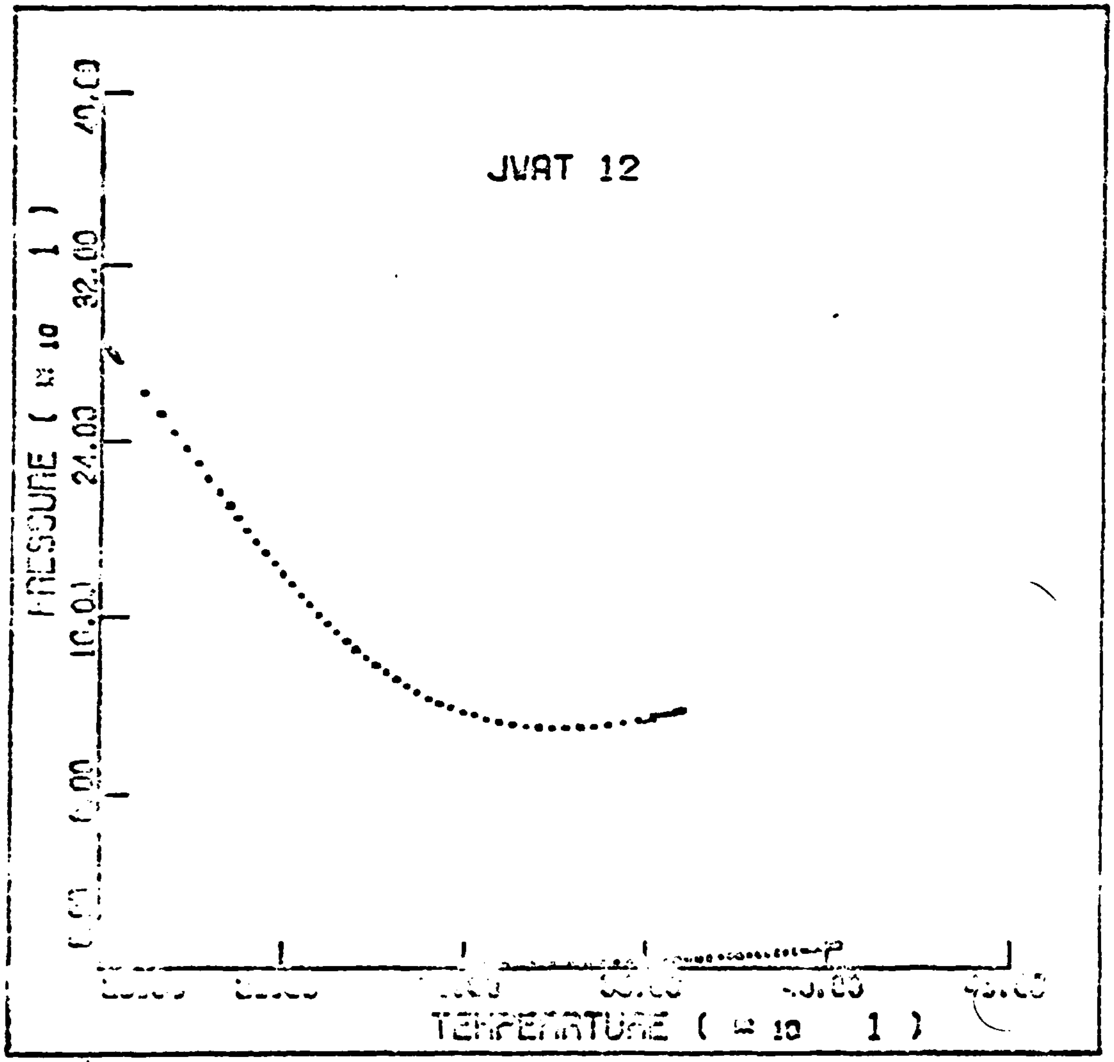
JVAT 12
PRESSURE (x 10 1)
40.00
32.00
24.00
16.01
0.00
TEMPERATURE (x 10 1)

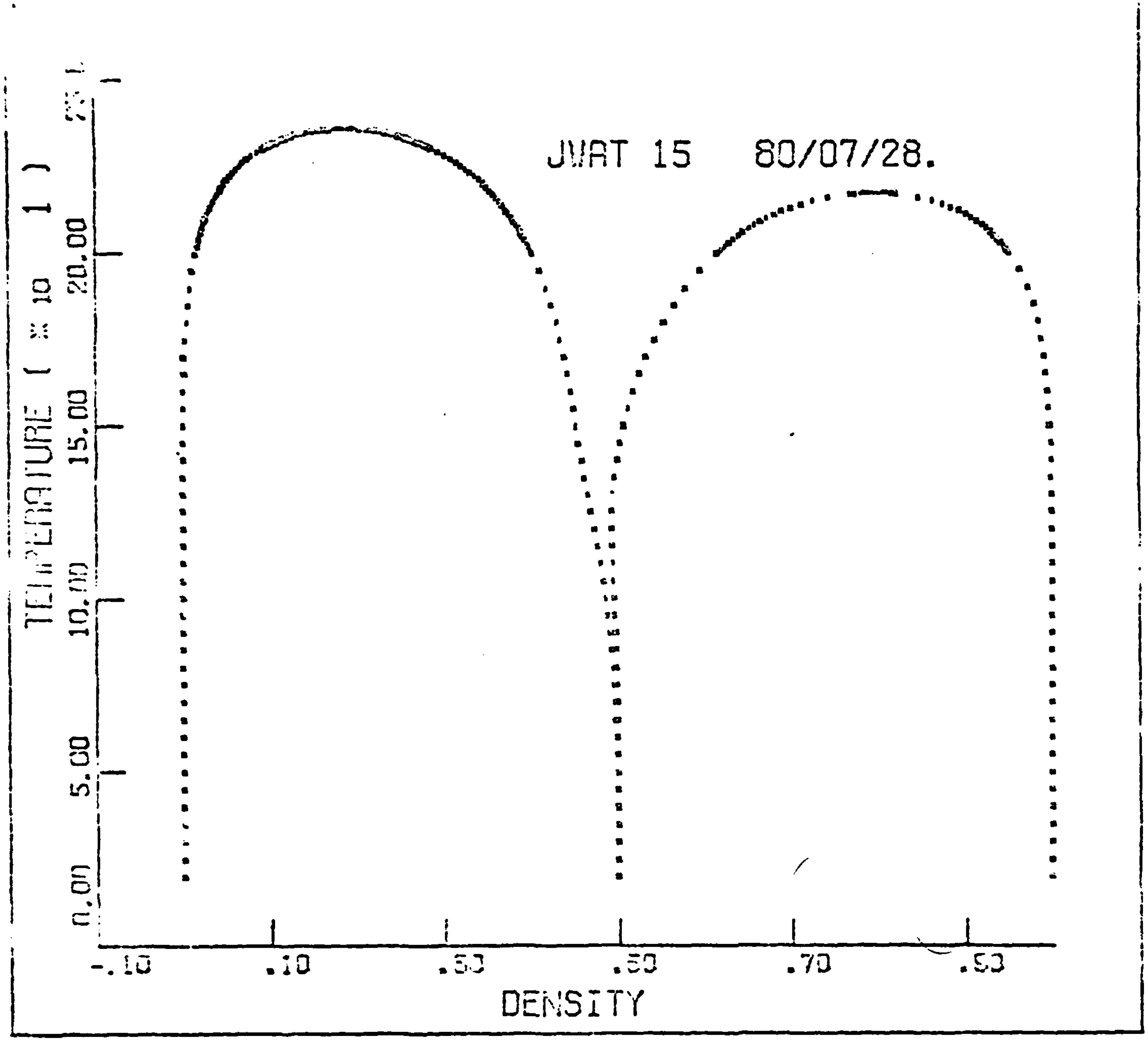
JWAT 15 80/07/28.
TEMPERATURE (× 10 1)
0.00
5.00
10.00
15.00
20.00
-.10
.10
.30
.50
.70
.90
DENSITY

F-6

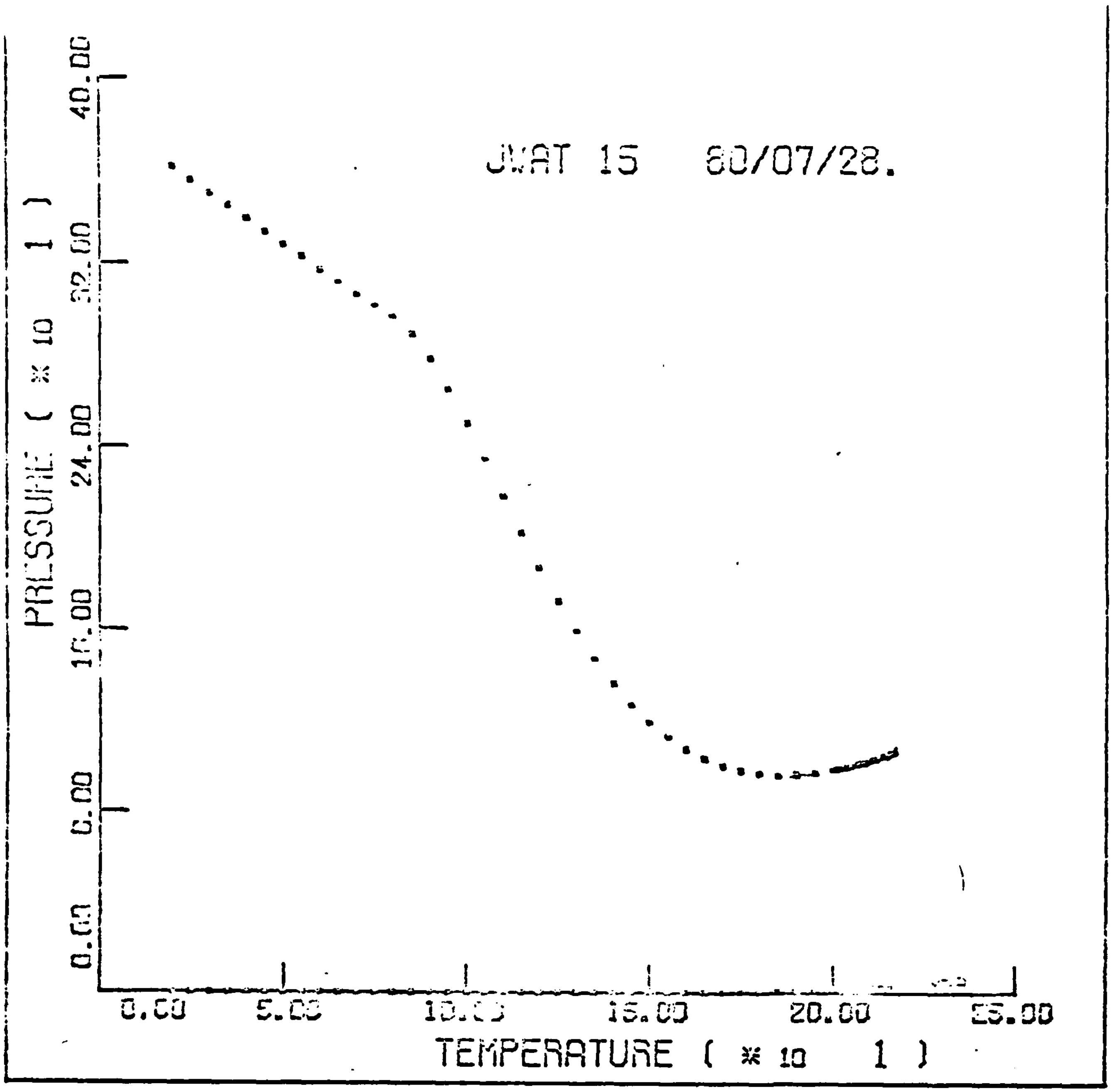
JWAT 15 80/07/28.
PRESSURE (* 10 1)
0.00
8.00
16.00
24.00
32.00
40.00
TEMPERATURE (* 10 1)
0.00
5.00
10.00
15.00
20.00
25.00

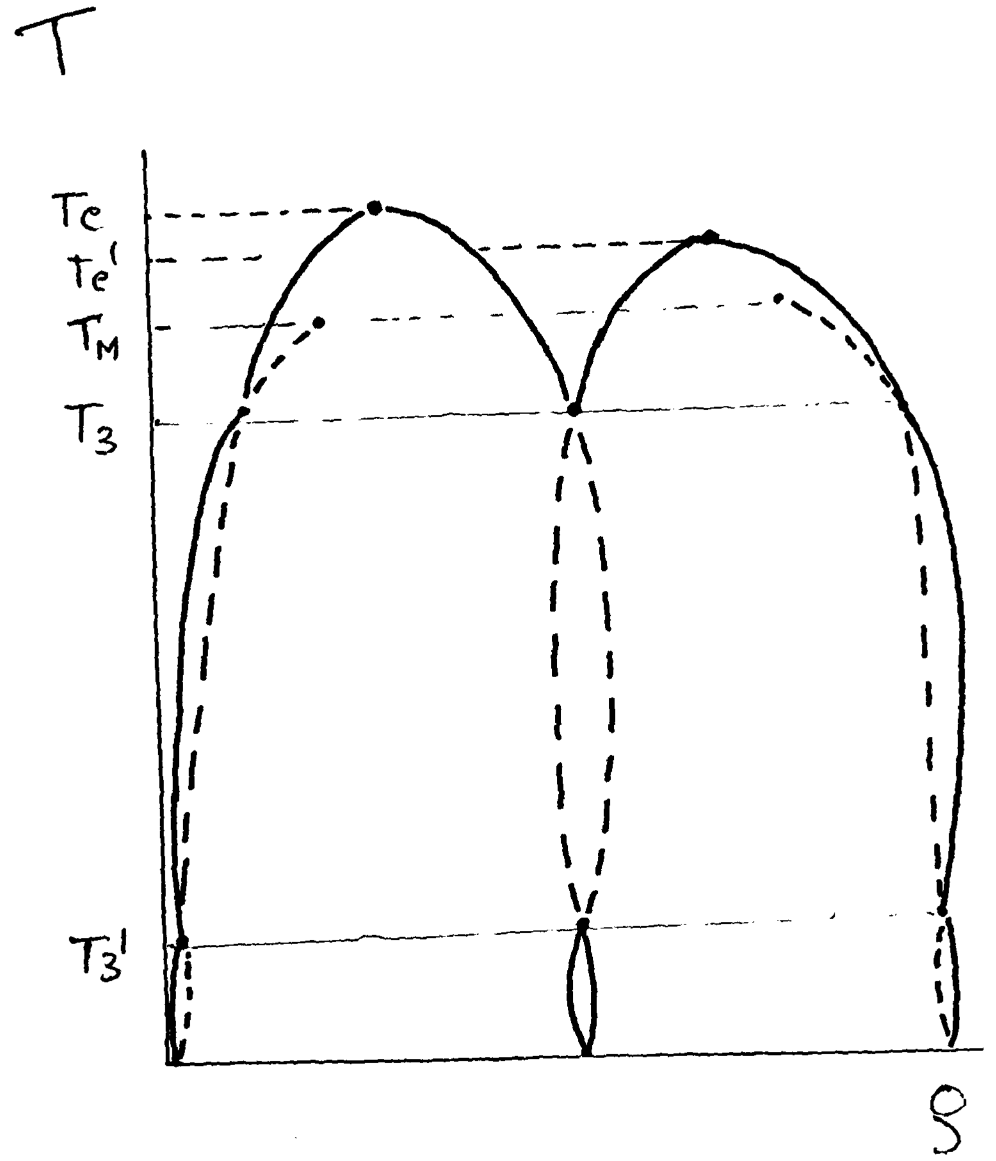

Fig 8

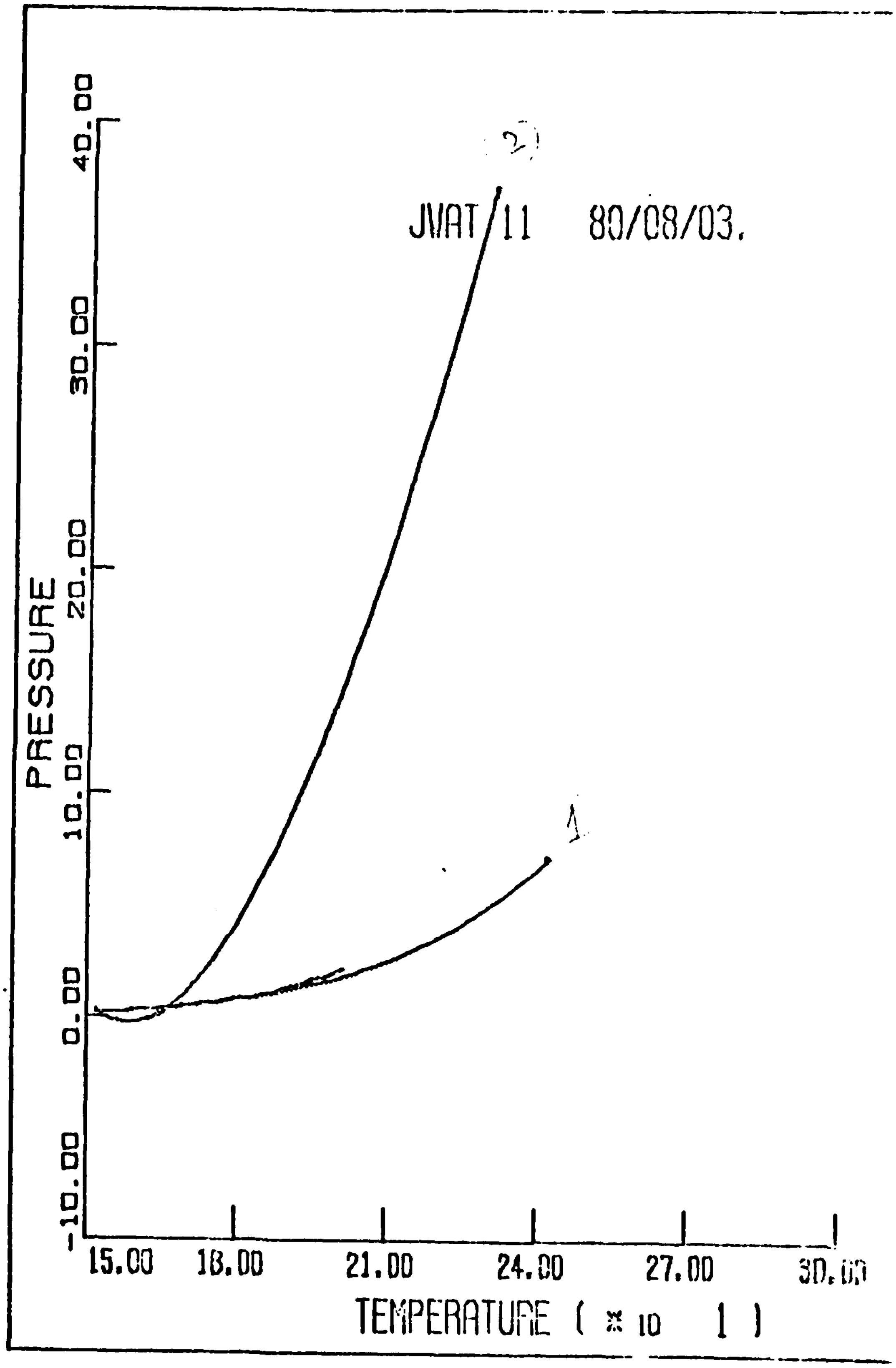
JVAT/11 80/08/03.
PRESSURE
40.00
30.00
20.00
10.00
0.00
-10.00
15.00
18.00
21.00
24.00
27.00
30.00
TEMPERATURE (* 10 1)
2)
1

Fig 9

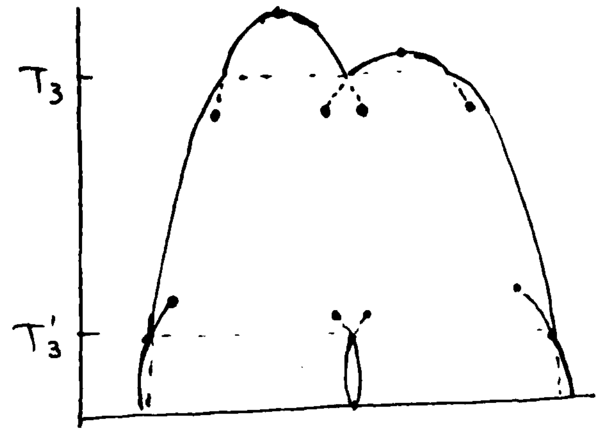

10 A

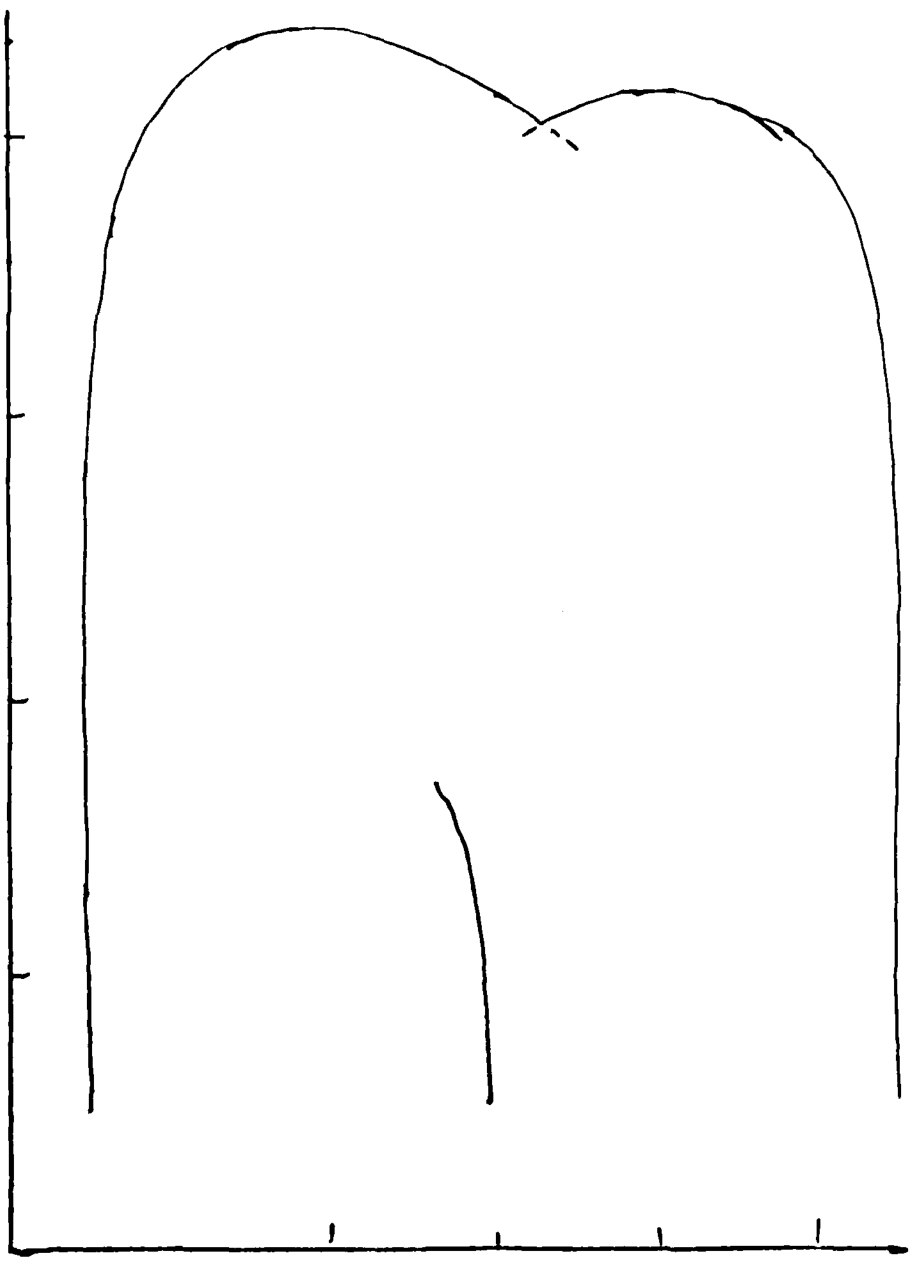

10 B

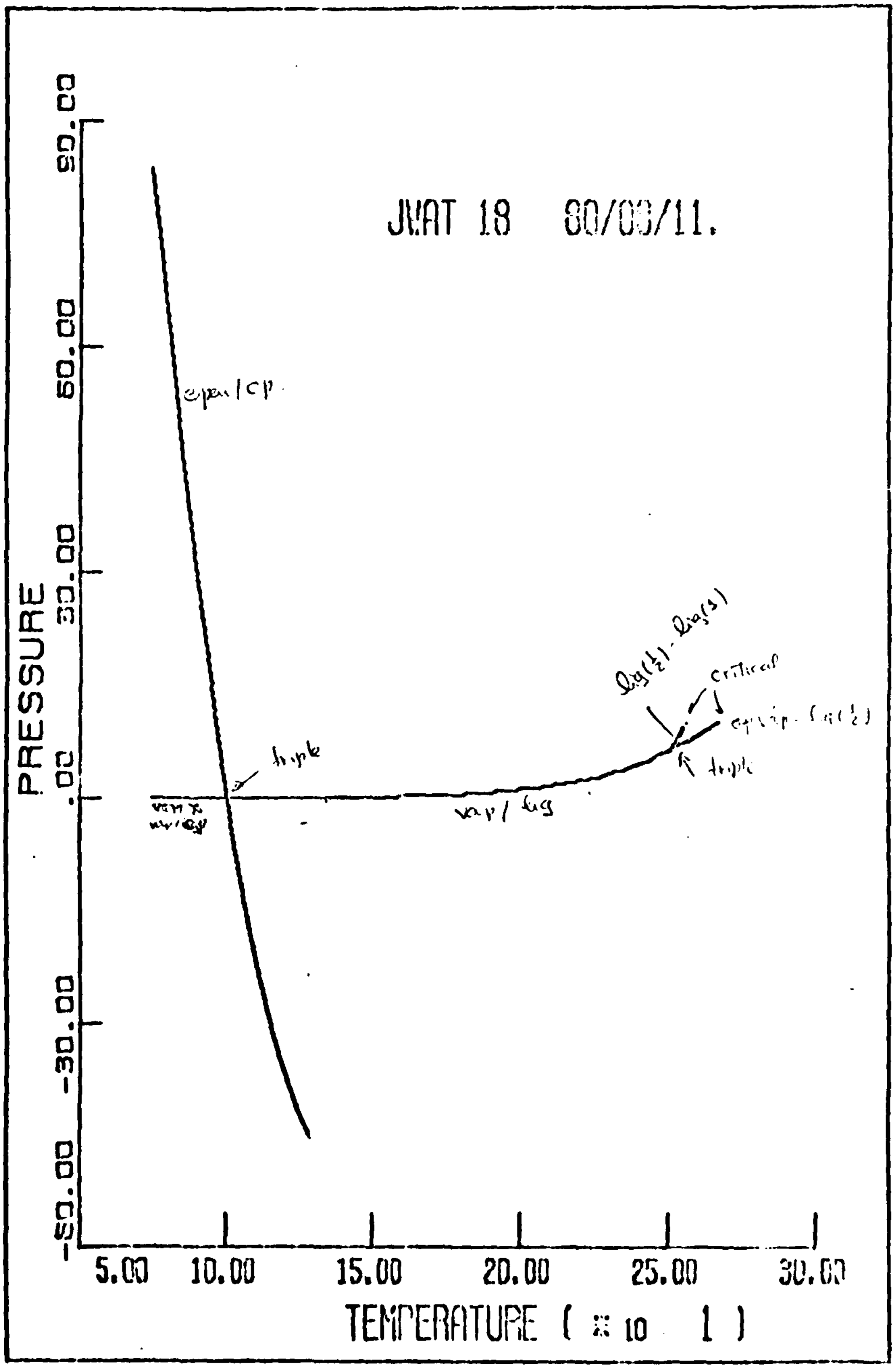
JVAT 1.8 80/03/11.
PRESSURE
TEMPERATURE (× 10 1)
90.00
60.00
30.00
.00
-30.00
-60.00
5.00
10.00
15.00
20.00
25.00
30.00
triple
critical
triple

Fig 11

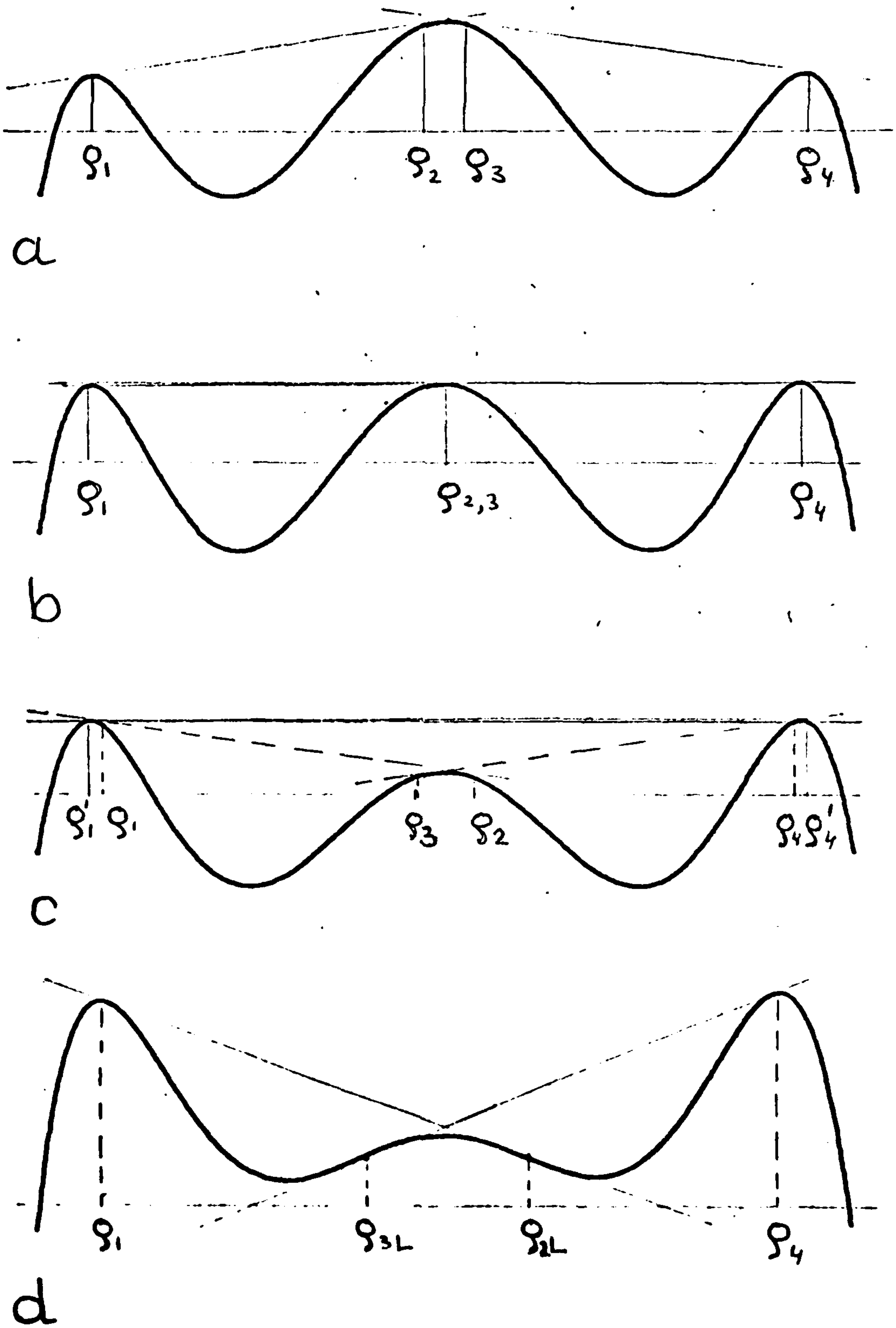
ρ_1
ρ_2
ρ_3
ρ_4
a
ρ_1
$\rho_{2,3}$
ρ_4
b
ρ_1'
ρ_1
ρ_3
ρ_2
ρ_4
ρ_4'
c
ρ_1
ρ_{3L}
ρ_{2L}
ρ_4
d

Fig 12

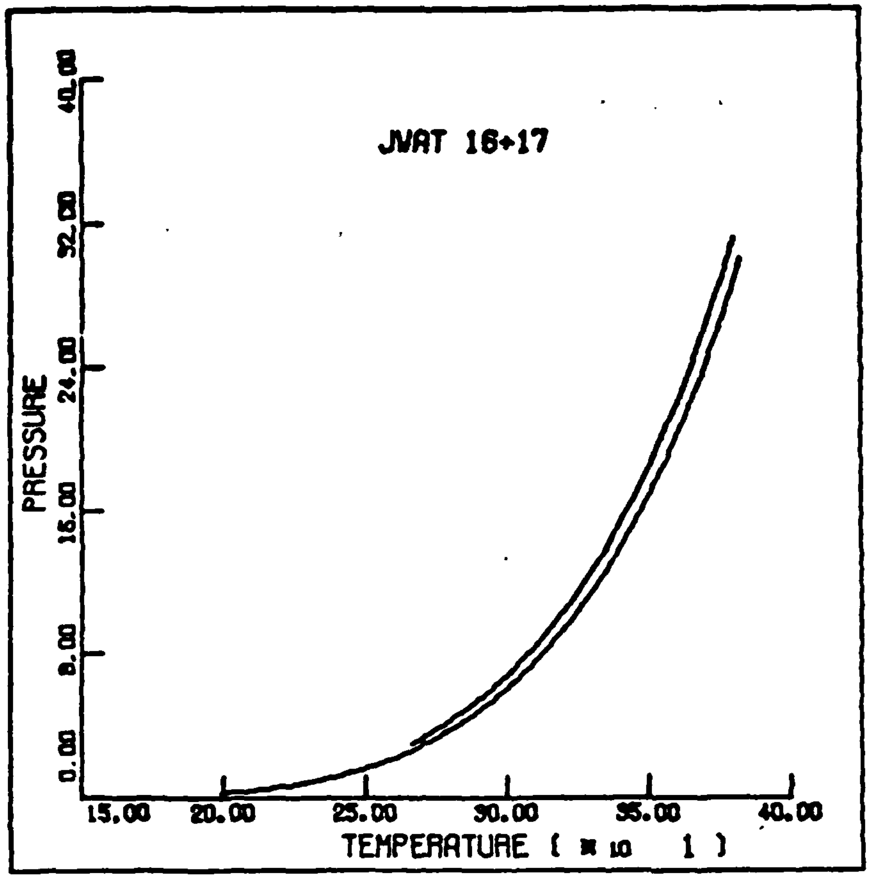

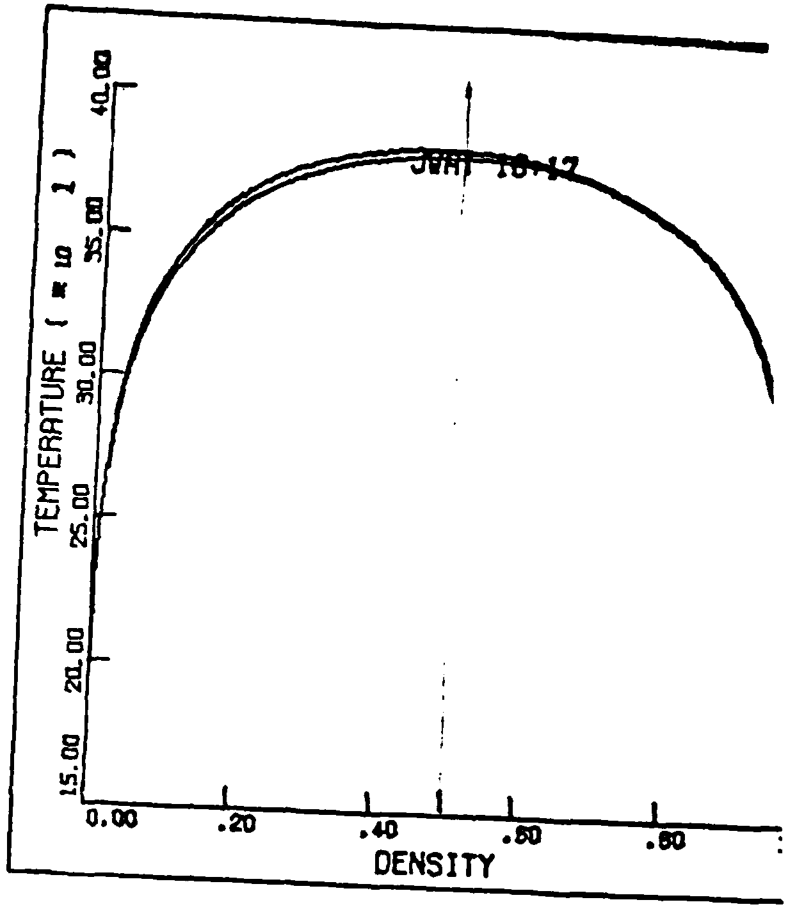

Fig 14

Fig 13

2/6/80

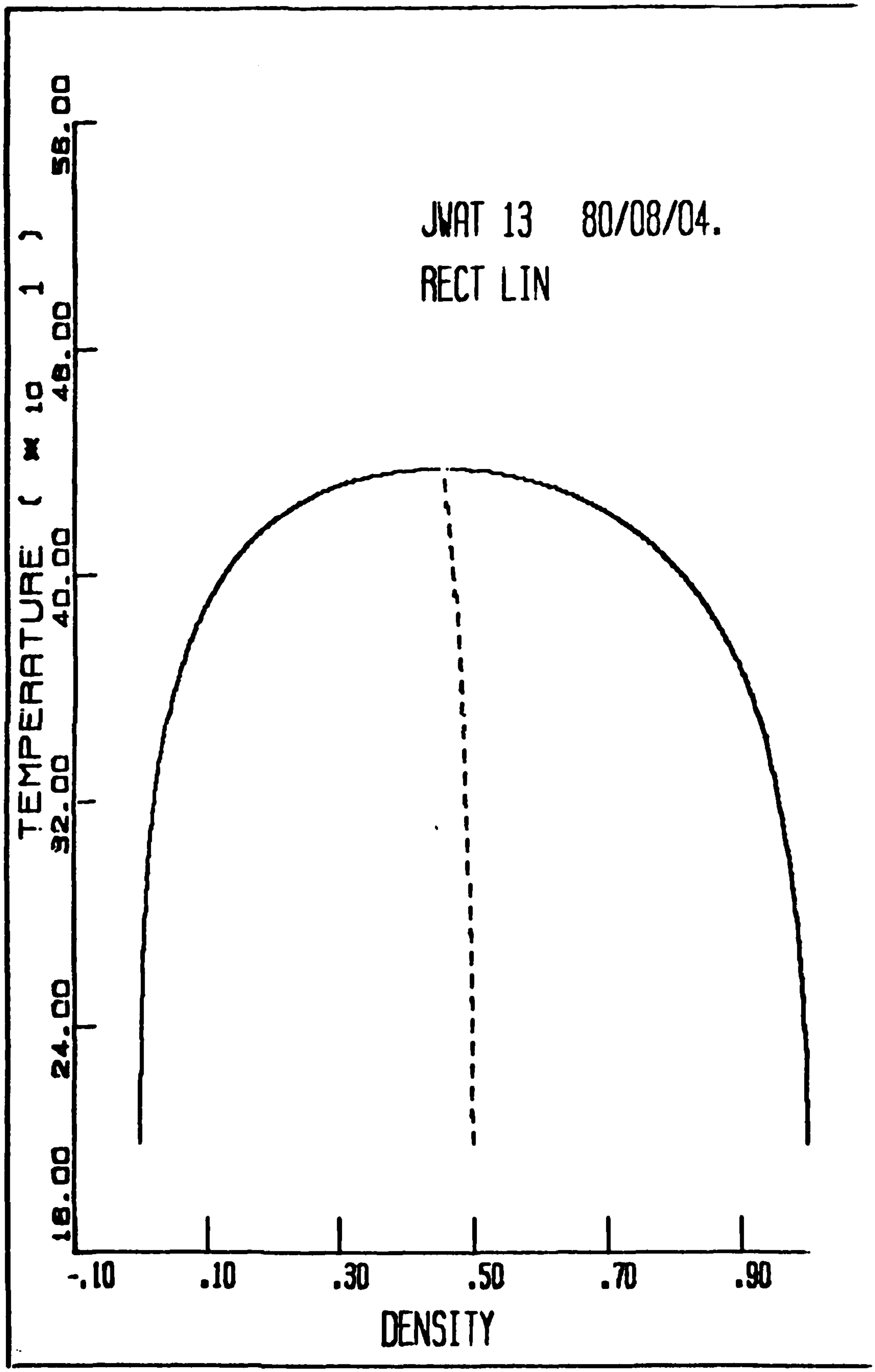
JWAT 13 80/08/04.
RECT LIN
TEMPERATURE (* 10 1)
56.00
48.00
40.00
32.00
24.00
16.00
-.10
.10
.30
.50
.70
.90
DENSITY

Fig 15

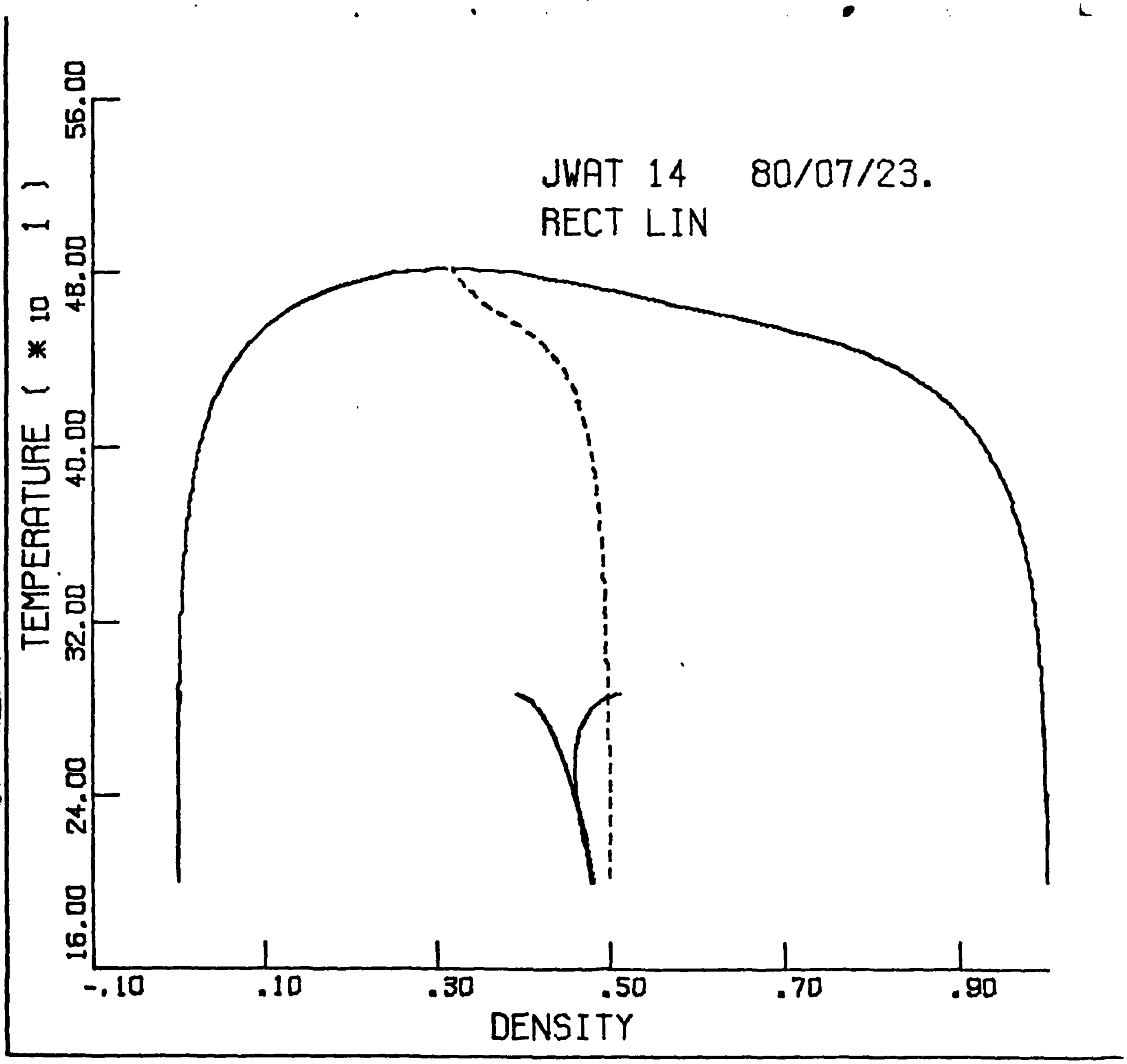

JWAT 14 80/07/23.
RECT LIN
TEMPERATURE (* 10 1)
56.00
48.00
40.00
32.00
24.00
16.00
-.10
.10
.30
.50
.70
.90
DENSITY

Fig 16

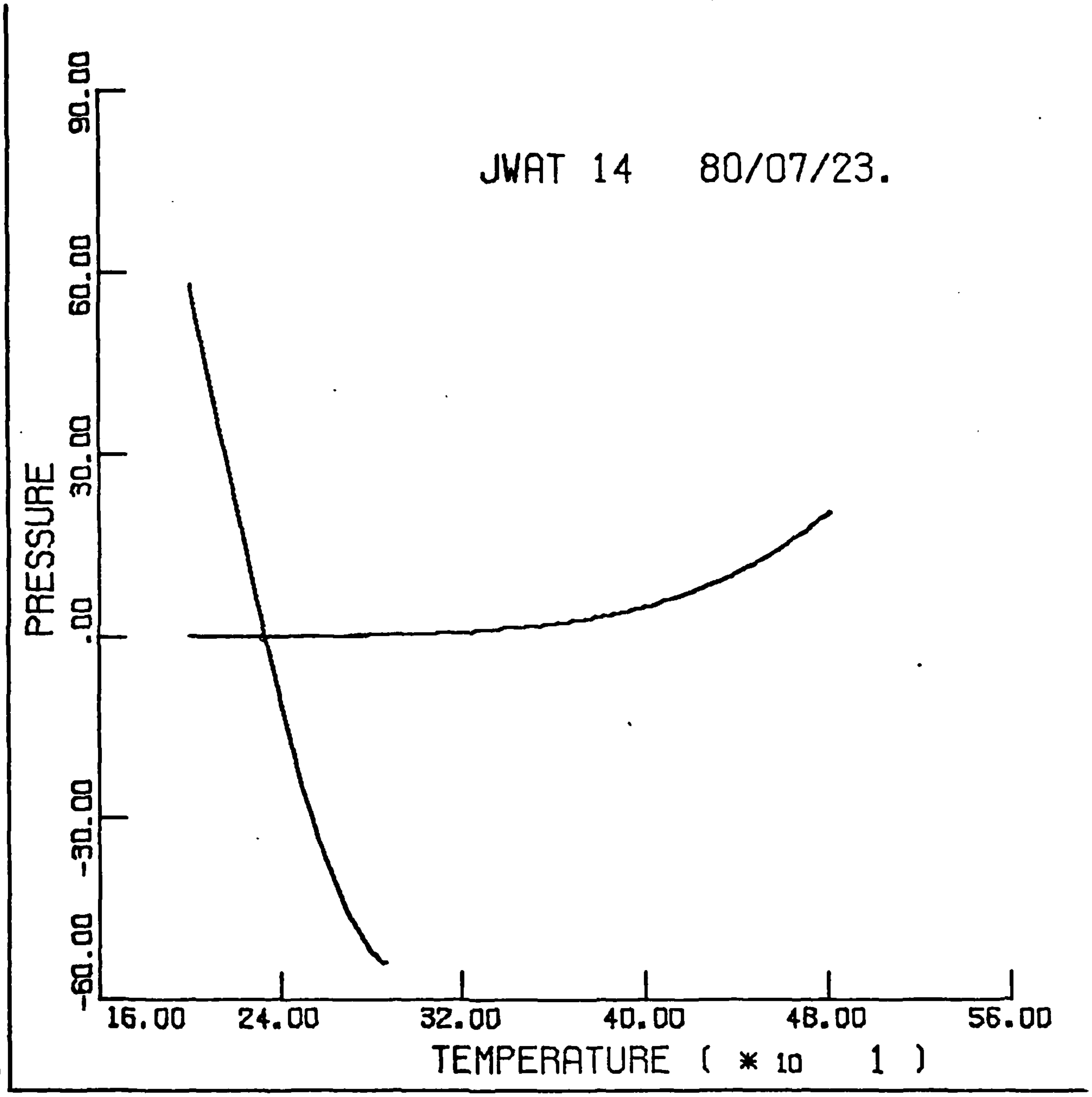
JWAT 14 80/07/23.
PRESSURE
90.00
60.00
30.00
.00
-30.00
-60.00
16.00
24.00
32.00
40.00
48.00
56.00
TEMPERATURE (* 10 1)

Fig 17

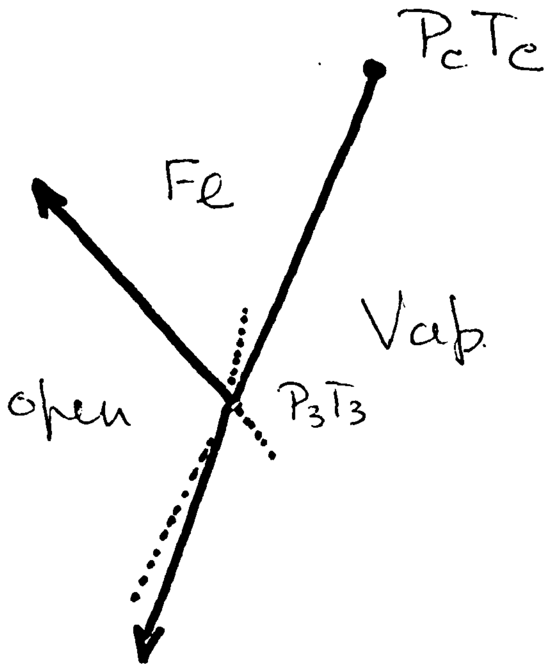

Fig 18

80/6/2

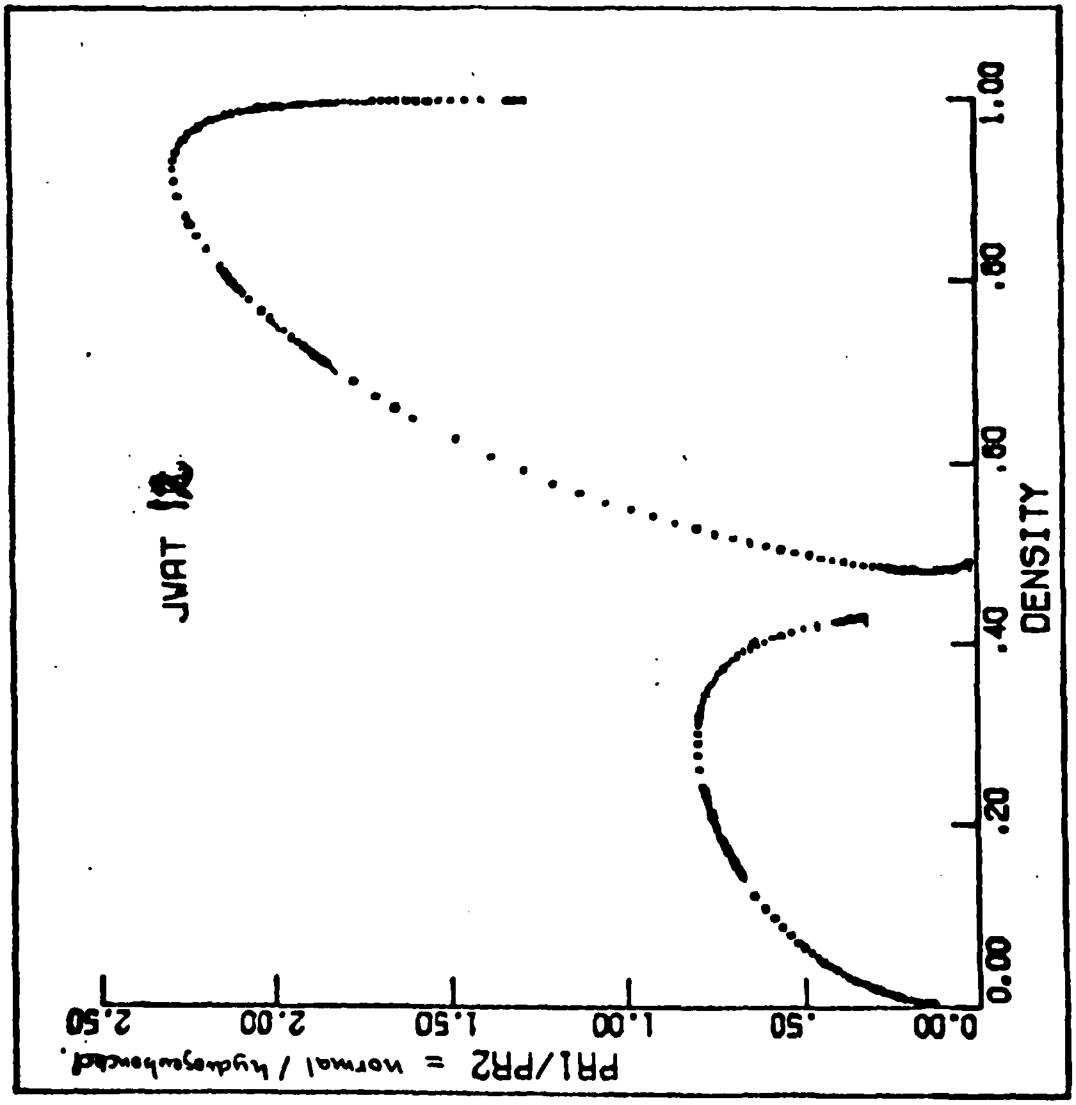

DENSITY
0.00
.20
.40
.60
.80
1.00
PR1/PR2 = normal / hydrogenated.
0.00
.50
1.00
1.50
2.00
2.50

Fig 19

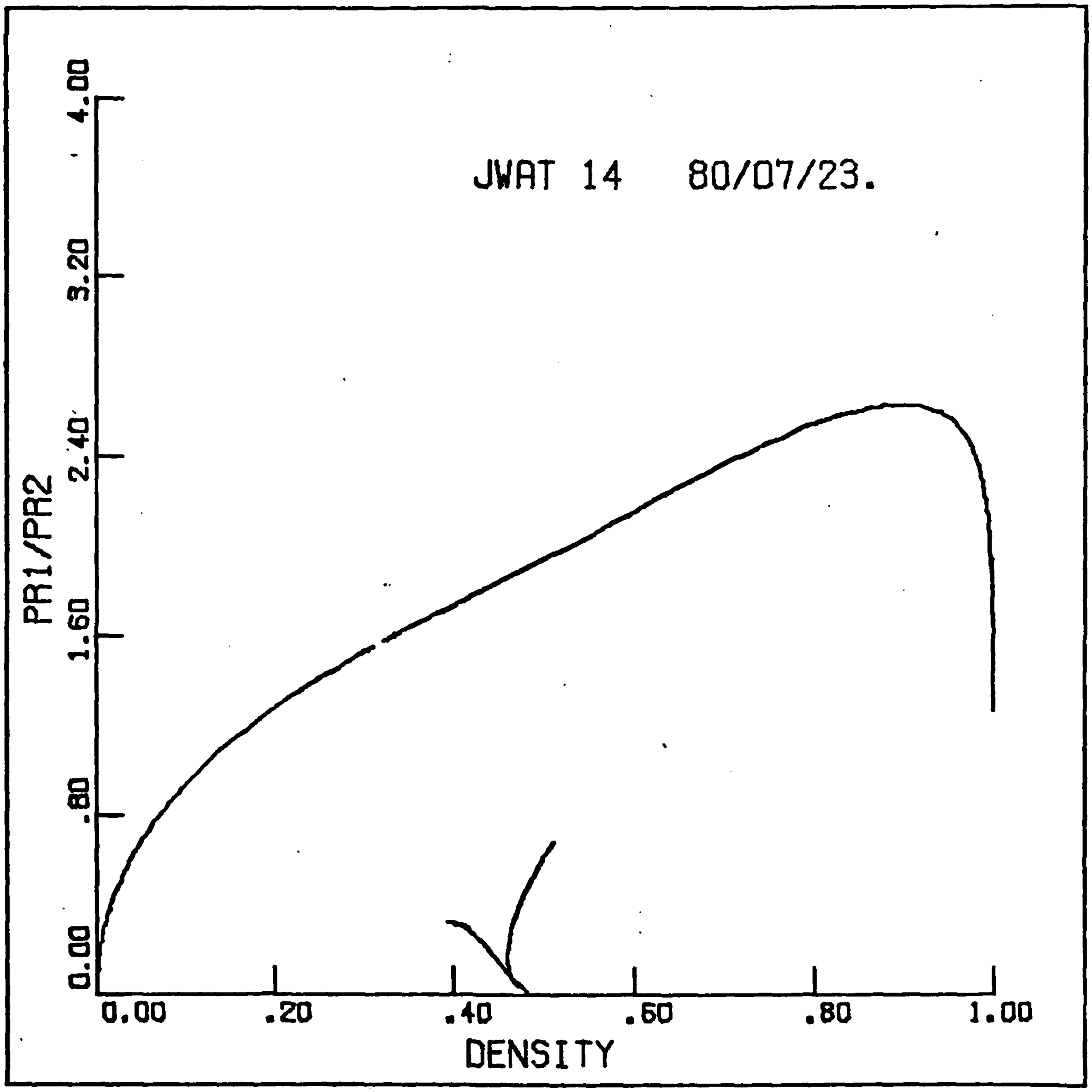
JWAT 14 80/07/23.
PR1/PR2
0.00
.80
1.60
2.40
3.20
4.00
0.00
.20
.40
.60
.80
1.00
DENSITY

Fig 20

TECHNICAL REPORT DISTRIBUTION LIST, GEN

	No. Copies
Office of Naval Research Attn: Code 472 800 North Quincy Street Arlington, Virginia 22217	2
ONR Branch Office Attn: Dr. George Sandoz 536 S. Clark Street Chicago, Illinois 60605	1
ONR Area Office Attn: Scientific Dept. 715 Broadway New York, New York 10003	1
ONR Western Regional Office 1030 East Green Street Pasadena, California 91106	1
ONR Eastern/Central Regional Office Attn: Dr. L. H. Peebles Building 114, Section D 666 Summer Street Boston, Massachusetts 02210	1
Director, Naval Research Laboratory Attn: Code 6100 Washington, D.C. 20390	1
The Assistant Secretary of the Navy (RE&S) Department of the Navy Room 4E736, Pentagon Washington, D.C. 20350	1
Commander, Naval Air Systems Command Attn: Code 310C (H. Rosenwasser) Department of the Navy Washington, D.C. 20360	1
Defense Technical Information Center Building 5, Cameron Station Alexandria, Virginia 22314	12
Dr. Fred Saalfeld Chemistry Division, Code 6100 Naval Research Laboratory Washington, D.C. 20375	1

	No. Copies
U.S. Army Research Office Attn: CRD-AA-IP P.O. Box 1211 Research Triangle Park, N.C. 27709	1
Naval Ocean Systems Center Attn: Mr. Joe McCartney San Diego, California 92152	1
Naval Weapons Center Attn: Dr. A. B. Amster, Chemistry Division China Lake, California 93555	1
Naval Civil Engineering Laboratory Attn: Dr. R. W. Drisko Port Hueneme, California 93401	1
Department of Physics & Chemistry Naval Postgraduate School Monterey, California 93940	1
Dr. A. L. Slafkosky Scientific Advisor Commandant of the Marine Corps (Code RD-1) Washington, D.C. 20380	1
Office of Naval Research Attn: Dr. Richard S. Miller 800 N. Quincy Street Arlington, Virginia 22217	1
Naval Ship Research and Development Center Attn: Dr. G. Bosmajian, Applied Chemistry Division Annapolis, Maryland 21401	1
Naval Ocean Systems Center Attn: Dr. S. Yamamoto, Marine Sciences Division San Diego, California 91232	1
Mr. John Boyle Materials Branch Naval Ship Engineering Center Philadelphia, Pennsylvania 19112	1

TECHNICAL REPORT DISTRIBUTION LIST, GEN

	No. Copies
Dr. Rudolph J. Marcus Office of Naval Research Scientific Liaison Group American Embassy APO San Francisco 96503	1
Mr. James Kelley DTNSRDC Code 2803 Annapolis, Maryland 21402	1

SP472-3/A27

472:GAN:716:ddc
78u472-608

TECHNICAL REPORT DISTRIBUTION LIST, 051B

	No. Copies
Professor K. Wilson Department of Chemistry, B-014 University of California, San Diego La Jolla, California 92093	1
Professor C. A. Angell Department of Chemistry Purdue University West Lafayette, Indiana 47907	1
~~Professor P. Meijer~~ ~~Department of Physics~~ ~~Catholic University of America~~ ~~Washington, D.C. 20064~~	1
Dr. S. Greer Chemistry Department University of Maryland College Park, Maryland 20742	1
Professor P. Delahay New York University 100 Washington Square East New York, New York 10003	1
Dr. T. Ashworth Department of Physics South Dakota School of Mines & Technology Rapid City, South Dakota 57701	1
Dr. G. Gross New Mexico Institute of Mining & Technology Socorro, New Mexico 87801	1
Dr. J. Kassner Space Science Research Center University of Missouri - Rolla Rolla, Missouri 65401	1
Dr. J. Telford University of Nevada System Desert Research Institute Lab of Atmospheric Physics Reno, Nevada 89507	1
Dr. B. Vonnegut State University of New York Earth Sciences Building 1400 Washington Avenue Albany, New York 12203	1
Dr. Hank Loos Laguna Research Laboratory 21421 Stans Lane Laguna Beach, California 92651	1
Dr. John Latham University of Manchester Institute of Science & Technology P.O. Box 88 Manchester, England M601QD	1